Nano Res (2009) 2: 373–379
DOI 10.1007/s12274-009-9036-5
Research Article

Simple and Rapid Synthesis of α-Fe_2O_3 Nanowires Under Ambient Conditions

Albert G. Nasibulin[1] (✉), Simas Rackauskas[1], Hua Jiang[1], Ying Tian[1], Prasantha Reddy Mudimela[1], Sergey D. Shandakov[1,2], Larisa I. Nasibulina[1], Jani Sainio[3], and Esko I. Kauppinen[1,4] (✉)

[1] NanoMaterials Group, Department of Applied Physics and Center for New Materials, Helsinki University of Technology, Puumiehenkuja 2, 02150, Espoo, Finland
[2] Laboratory of Carbon NanoMaterials, Department of Physics, Kemerovo State University, Kemerovo 650043, Russia
[3] Laboratory of Physics, Helsinki University of Technology, Otakaari 1 M, 02150, Espoo, Finland
[4] VTT Biotechnology, Biologinkuja 7, 02044, Espoo, Finland

Received: 16 January 2009 / Revised: 24 February 2009 / Accepted: 1 March 2009

ABSTRACT
We propose a simple method for the efficient and rapid synthesis of one-dimensional hematite (α-Fe_2O_3) nanostructures based on electrical resistive heating of iron wire under ambient conditions. Typically, 1–5 μm long α-Fe_2O_3 nanowires were synthesized on a time scale of seconds at temperatures of around 700 °C. The morphology, structure, and mechanism of formation of the nanowires were studied by scanning and transmission electron microscopies, energy dispersive X-ray spectroscopy, X-ray photoelectron spectroscopy, and Raman techniques. A nanowire growth mechanism based on diffusion of iron ions to the surface through grain boundaries and to the growing wire tip through stacking fault defects and due to surface diffusion is proposed.

KEYWORDS
Fe_2O_3, hematite, mechanism, nanowire, synthesis

One-dimensional semiconducting nanostructured oxides in the form of wires have recently attracted tremendous attraction due to their novel properties [1–7]. Hematite (α-Fe_2O_3) is one of the most interesting and important metal oxides. It is an n-type semiconductor with a band gap of 2.1 eV and has antiferromagnetic properties [8]. Hematite is known to catalyze a number of chemical reactions and due to its low toxicity can be successfully employed in many chemical and biochemical applications [9–12]. In addition, α-Fe_2O_3 has many other uses including in nonlinear optics, gas sensors, and as a pigment [13–15].

The growth of α-Fe_2O_3 nanowires (NWs) has been carried out mainly on pure iron foils/plates or powder in a heated and well-controlled environment, i.e., at a certain partial pressure of particular gases or under vacuum conditions [13, 16–22]. Typical time required for the synthesis of a dense NW "forest" by oxidation of pure iron range from hours to a few tens

Address correspondence to A. Nasibulin, albert.nasibulin@hut.fi; E. Kauppinen, esko.kauppinen@tkk.fi

of hours. Recently, a new way of rapid NW synthesis by direct plasma oxidation of bulk materials was proposed [23, 24]. However, this method is complicated, since it requires both vacuum conditions and equipment to create plasma under controlled conditions. Here, we propose a very simple method, which does not require any complicated equipment or a controlled atmosphere, since the synthesis can be carried out using a basic DC power supply (such as a car battery or a set of household batteries) under ambient conditions; the process of NW formation is very rapid, with a typical growth time of a few seconds, and with a very little energy consumption. The method is described in detail in the Electronic Supplementary Material (ESM).

In spite of intensive research into one-dimensional structures of metal oxides in particular and NWs in general, our understanding of the mechanisms of their formation and growth is still incomplete. Our method affords the possibility to investigation the NW growth. The morphology, structure, and nanowire formation were examined by scanning and transmission electron microscopies (SEM and TEM), energy dispersive X-ray spectroscopy (EDX), X-ray photoelectron spectroscopy (XPS), and Raman techniques.

Iron oxide NWs were grown by resistive heating of iron wire (99.99% and 99.5%, Goodfellow) with a diameter of 0.25 mm under ambient laboratory conditions. The growth was carried out by applying a potential difference of 2.7–7.8 V (with a current of 2.5–2.6 A) to 5.8–15.0 cm long Fe wires. It is important to note that the synthesis can be easily controlled by observing the color of the wire and by varying the applied heating power (see the ESM). SEM observation of the wire after the synthesis of the reddish material revealed that the wire was completely covered by NWs (Fig. 1). The NWs had a sword-like shape, i.e., they are belt-like structures, which are thicker at the base and thinner at the end. EDX analysis confirmed that the NWs consisted of oxygen and iron (see ESM). A bright-field TEM image (Fig. 2(a)) showed that typical length of the NWs was about 1–5 μm. High-resolution TEM images (with their Fourier transform shown as an inset) were consistent with the rhombohedral crystal structure of α-Fe_2O_3 (Fig. 2(b) and ESM). A tilt series of electron diffraction patterns from an individual NW (Fig. 2(c)) obtained by rotating the wire around its axis at 0°, 32.5°, and 50.2° were indexed as zone axes of [001] (Fig. 2(d)), [−111] (Fig. 2(e)), and [−221] (Fig. 2(f)) of rhombohedral α-Fe_2O_3. Thereby, based on the TEM analysis it can be concluded that the NWs grow in the [110] direction, which is in agreement with the literature [21]. Detailed TEM investigations showed that the NWs are single-crystalline with stacking faults oriented along the wires (see ESM).

In order to confirm the formation of an α-Fe_2O_3 phase we carried out XPS measurements. The binding energy scale was referenced to the characteristic carbon 1s binding energy of 285 eV (Fig. 3(a)). The Fe $2p_{3/2}$ maximum was found at approximately 710 eV and the first satellite peak at 719 eV (Fig. 3(b)). The positions of these peaks as well as the shape of the Fe 2p spectrum agree well with those for the Fe^{3+} state reported in Ref. [25]. The presence of two states of

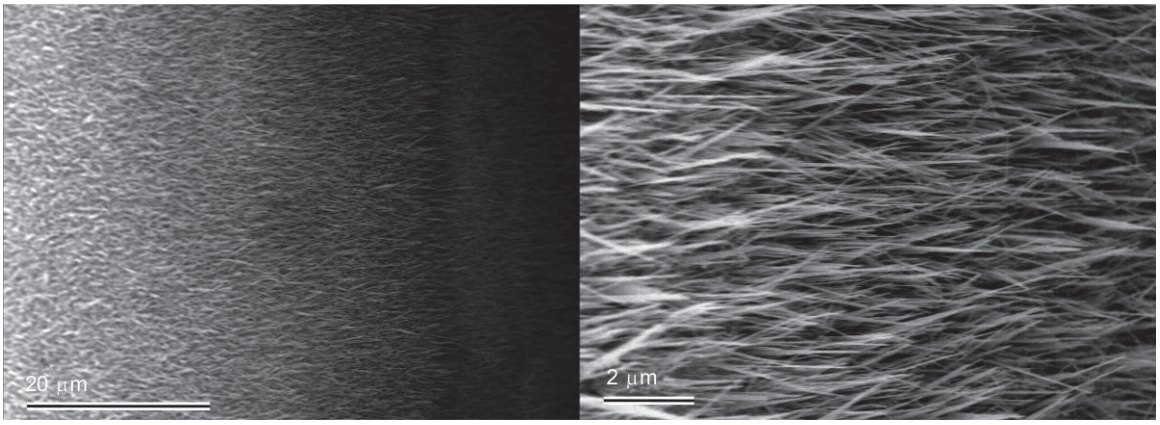

Figure 1 SEM images of the surface of the iron wire after the synthesis

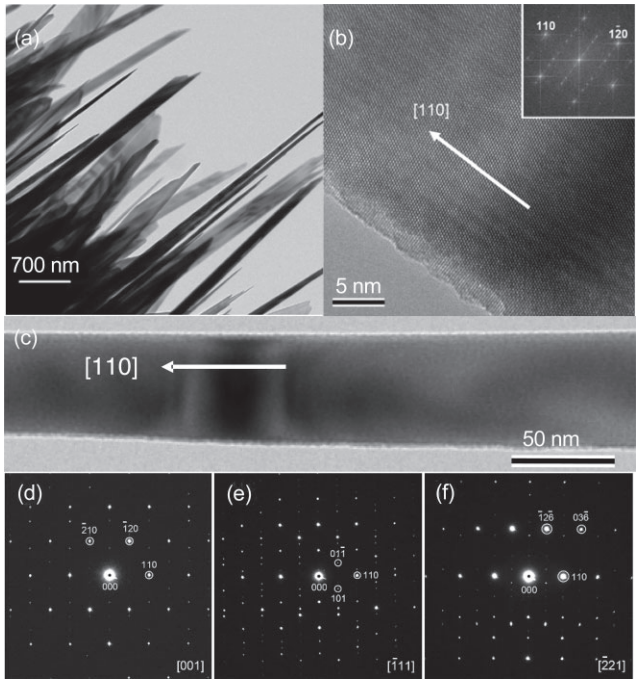

Figure 2 TEM images of NWs at (a) low and (b) high magnifications. The inset in (b) shows the Fourier transform indexed as α-Fe_2O_3. (c) TEM image of an individual NW. (d)–(f) A tilt series of electron diffraction patterns obtained by rotating the NW along its axis by (e) 32.5° and (f) 50.2° from pattern (d)

oxygen in the samples is shown in Fig. 3(c). The main peak at 529.5 eV most likely corresponds to O^{2-} in the iron oxide lattice. The second broad feature is shifted by about 2 eV to higher binding energy and can be attributed to OH^- or adsorbed oxygen [26]. Thus, the XPS analysis confirmed the formation of a Fe_2O_3 phase.

Raman investigations of the cross-section part of the wire revealed the formation of different layers during the NW growth (Figs. 4(a) and 4(b)). The spectra showed that the upper layer of the wire consists of mainly α-Fe_2O_3 as can be seen in Fig. 4(c). In addition to Raman peaks corresponding to α-Fe_2O_3 (at 225, 245, 292, 411, 498, 611, and 1323 cm^{-1}), a very weak peak of Fe_3O_4 at 663 cm^{-1} [27, 28] was also detected in the surface layer of the oxidized wire. The next layer can be clearly distinguished in SEM and optical and SEM images in Figs. 4(a) and 4(b) and was assigned to Fe_3O_4 (on the basis of the Raman peaks at 299, 537, and 633 cm^{-1} in Fig. 4(d)) [28]. This layer was found to be fairly porous. The third layer is about 10 μm thick and gives the only peak at 645 cm^{-1} corresponding to FeO (Fig. 4(e)). Spectra from the core of the iron wire under the oxide layers, which were peeled off, did not show any Raman signal, which suggests that the core consists of a pure iron phase. These results show that the oxidation state of iron increases from 0 to +3 on going from the core to the upper layer.

As mentioned above, the growth of α-Fe_2O_3 NWs is generally a time-consuming process [13, 16–22]. Our method, based on rapid wire heating from ambient temperature to the optimum synthesis temperature allowed us to determine the maximum NW growth rate. For this purpose, we applied a potential difference to wires (to heat them up to 700 °C) for a certain period of time (the growth time). After this time, the wires were rapidly cooled down by switching the power off. Surprisingly, after only 2 s growth time, α-Fe_2O_3 NWs with a length of about 200 nm were already found on the surface of the treated wires (see ESM). Thus, it can be concluded that the growth of α-Fe_2O_3 NWs is a rapid process with the growth rate exceeding 100 nm/s. A very dense NW forest was produced after 40 s and no significant changes were observed when heating time was further increased. This rapid NW growth is

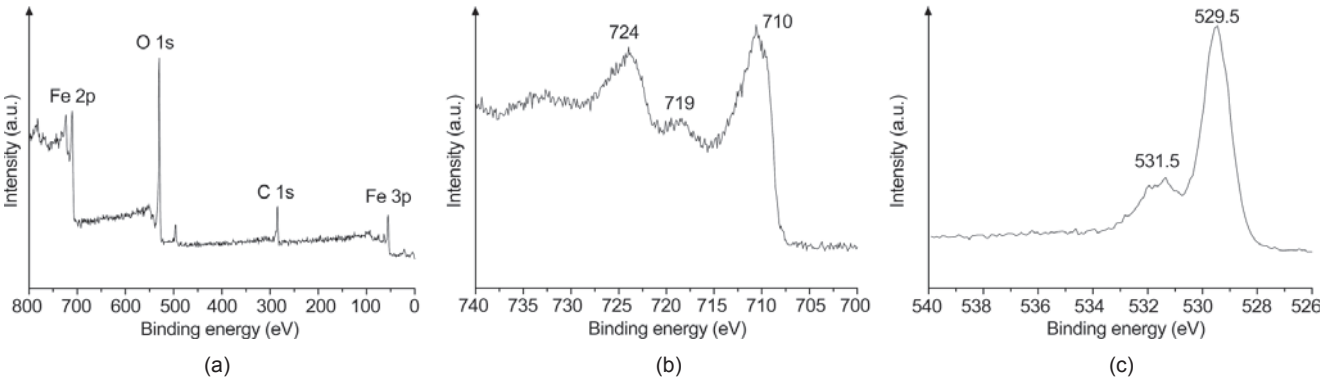

Figure 3 XPS spectra of α-Fe_2O_3 NWs: (a) wide range spectrum; (b) Fe 2p spectrum; (c) O 1s spectrum

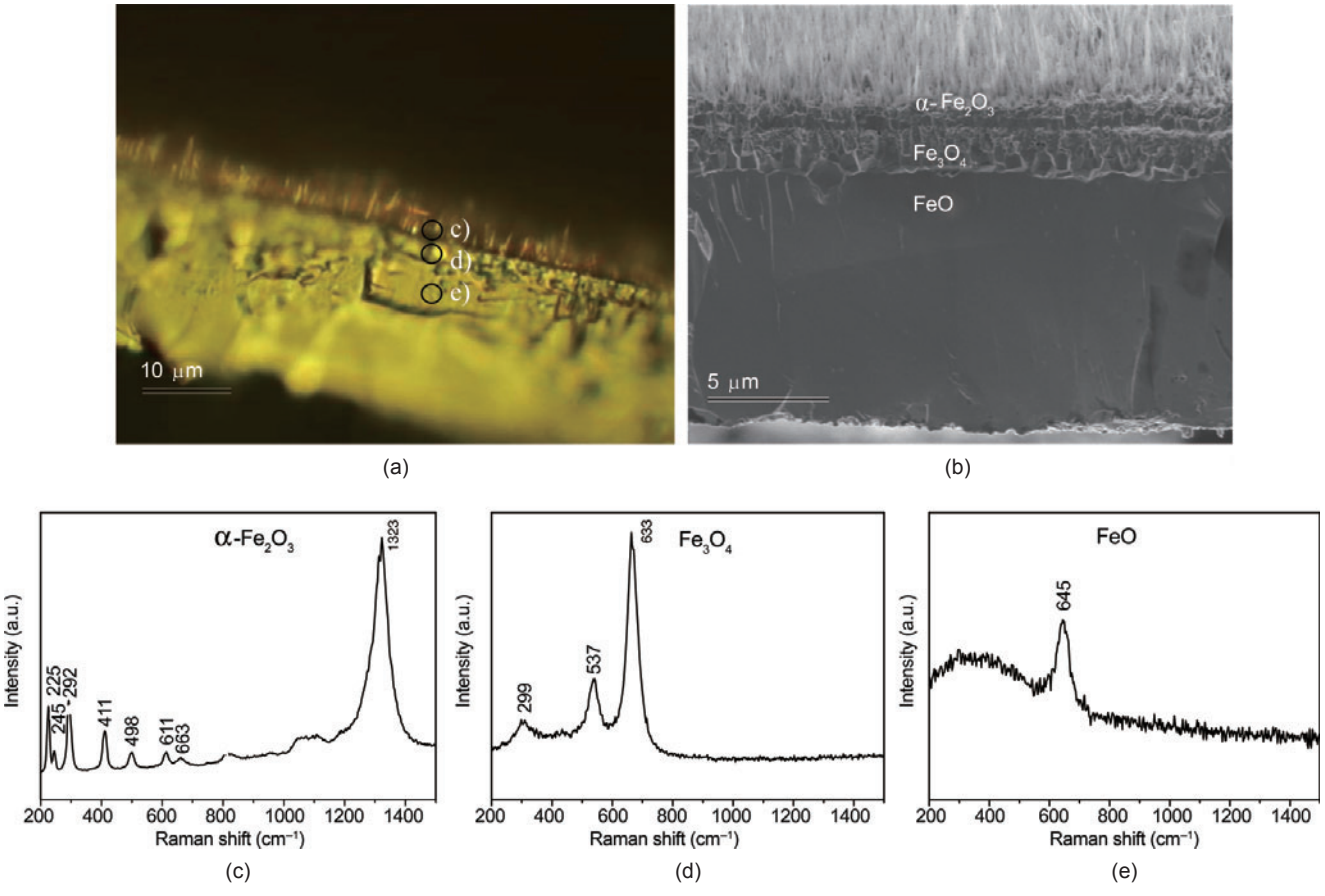

Figure 4 Iron oxide layers: (a) optical microscope image (circles indicate approximate areas of Raman measurements); (b) SEM image showing different iron oxidation layers. Raman spectra of iron oxide layers from the indicated measurement points: (c) α-Fe_2O_3, (d) Fe_3O_4, (f) FeO

observed in the temperature "window" from 700 to 720 °C.

The enhanced growth at temperatures of around 700 °C coincides with the results observed by Takagi [22]. However, in our case the growth rate is about one order of magnitude higher than the maximum rate in an oxygen atmosphere reported by Takagi. This can be explained by the different heating speeds and temperature profiles across the wires: in our method the wire was rapidly heated from below the surface, providing a higher temperature gradient across the wire compared to that obtained with conventional furnace oxidation techniques. Another important reason is the presence of water and CO_2 in ambient air, which can increase the rates of formation and growth of NWs [29].

NW growth is usually described by either vapor–solid or vapor–liquid–solid mechanisms [30–36]. In our case, the NW synthesis occurred at low temperatures (significantly lower than the melting temperatures of both iron and its oxides) and at negligibly small equilibrium pressures of iron vapor above pure metal or its oxides and therefore cannot be ascribed to any of these mechanisms. NW growth during iron oxidation has also been explained by the stress driven mechanism [13, 17, 20–22], in which a relaxation of the large stress results in NW formation generated by dislocation slips. Substantial stresses are expected to be accumulated on the interface due to structural and density differences [17]. In the stress driven mechanism, it is believed that the upper layer provides a path to release the stress in the form of NWs. However, simple estimations of the density of different oxide layers show that the volume increase in the FeO layer is 77% with respect to Fe, the volume of Fe_3O_4 shows a 255% increase with respect to FeO, while the formation of Fe_2O_3 is accompanied by a 32% decrease in the molecular volume. This means that the stress should be mainly accumulated in the Fe_3O_4 and FeO layers and cannot directly affect the

growth of the NWs.

Figure 5 shows our understanding of the NW formation conditions and a suggested mechanism for their growth on the basis of our experimental results and literature data. The formation of NWs occurs when three layers of iron oxides are gradually formed by oxidation of iron. We believe that the growth of NWs is determined by diffusion processes. The driving force determining the motion of iron and oxide ion species is the potential difference appearing during the wire oxidation process. The electric field strength between iron and Fe_2O_3 layers can reach values as large as 10^6 V/cm [37]. It is worth noting that the electric field arising during resistive heating of an iron wire is about six orders of magnitude lower and thereby cannot significantly affect the ion motion across the wire. The iron oxidation process involves iron ion diffusion from the iron wire core to the surface through the iron oxide layers and diffusion of oxide ions in the opposite direction [37, 38]. At certain temperatures, grain boundaries in the FeO and Fe_3O_4 layers, likely formed due to the oxidation stress, could be responsible for higher diffusion rates compared to lattice diffusion [38]. In the initial stage, the Fe_2O_3 phase might grow in all directions; however, further growth only occurs in the [110] crystallographic direction as this is energetically most favorable [21], involving easier diffusion and favorable stacking. It is worth noting that the presence of stacking faults in the growth direction supports our proposed mechanism, since the diffusion rate is enhanced in crystal defects at elevated temperatures [39, 40]. Another path for iron ion delivery to the top of the growing NW is surface diffusion. The sword-like shape of the NWs confirms that the growth is determined by a diffusion process from the bottom—where the NWs are thicker—to the top, where they become thinner.

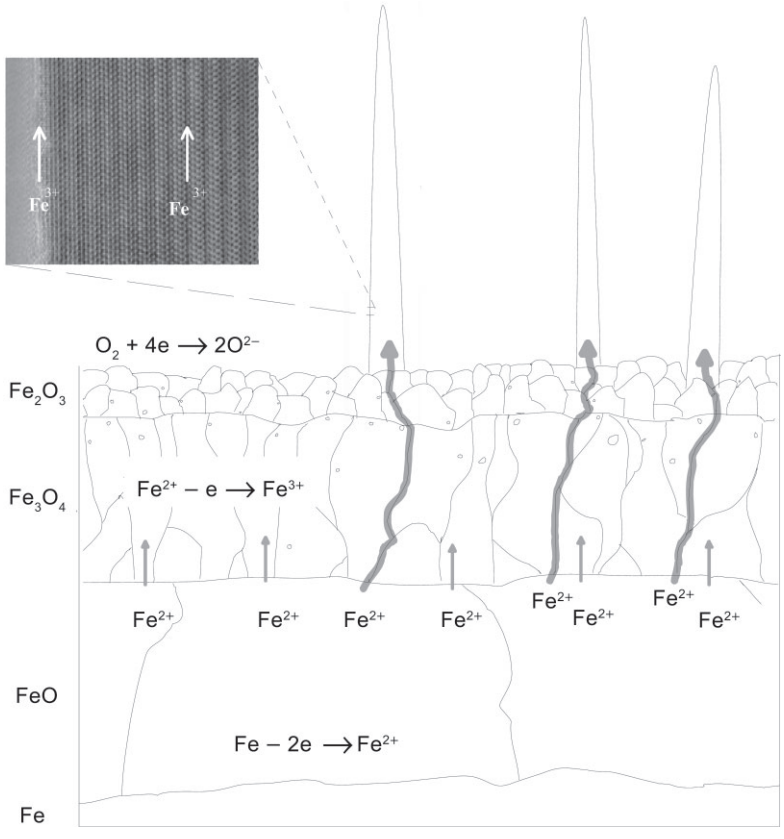

Figure 5 Schematic presentation of the NW growth in ambient air: delivery of iron ions through grain boundaries to the surface and the growth of NWs via diffusion through stacking fault defects in the [110] direction and surface diffusion

In conclusion, we propose a very simple method based on resistive heating of iron wires under ambient laboratory conditions to synthesize 1-D hematite (α-Fe_2O_3) nanostructures in the form of NWs with a length of 1–5 μm. It was shown that the iron wire after heat treatment consisted of layers of different iron-containing compounds starting from Fe in the core via FeO and Fe_3O_4 to Fe_2O_3 on the surface. The most efficient growth of α-Fe_2O_3 with a high density on the surface of the iron wire was found at temperatures of about 700 °C. Formation of NWs was detected even after 2 s. The NW growth rate was estimated to exceed 100 nm/s, which is about one order of magnitude higher than the maximum rate reported previously. It was found that NWs grew in the [110] crystallographic direction and contained stacking faults along the NW direction. A mechanism of NW growth based on the diffusion of iron ions to the surface of wire through grain boundaries and to the tip of the growing NW through stacking faults and by surface diffusion is proposed.

Acknowledgements

The authors thank Dr. Paula Queipo for investigations of the iron oxide NW stability. This work was supported by the Academy of Finland (project numbers 128445 and 128495). P. R. M. acknowledges Finnish National Graduate School in Nanoscience (NGS-NANO). S. D. S. thanks the European Commission for financial support through a Marie Curie Individual Fellowship (MIF1-CT-2005-022110).

Electronic Supplementary Material: Supplementary material is available in the online version of this article at http://dx.doi.org/10.1007/s12274-009-9036-5 and is accessible free of charge. (1) Growth of nanowires; (2) Nanowires: Six years later; (3) TEM investigations of nanowires; (4) Kinetics of nanowire growth.

References

[1] Li, Y.; Qian, F.; Xiang, J.; Lieber, C. M. Nanowire electronic and optoelectronic devices. *Mater. Today* **2006,** *9,* 18–27.

[2] Lu, J. G.; Chang, P.; Fan, Z. Quasi-one-dimensional metal oxide materials—Synthesis, properties and applications. *Mater. Sci. Eng. R* **2006,** *52,* 49.

[3] Fang, X.; Zhang, L. One-dimensional ZnS nanomaterials and nanostructures. *J. Mater. Sci. Technol.* **2006,** *22,* 721.

[4] Law, M.; Goldberger, J.; Yang, P. Semiconductor nanowires and nanotubes. *Ann. Rev. Mater. Res.* **2004,** *34,* 83–122.

[5] Kolasinski, K. W. Current opinion in solid state and materials. *Science* **2006,** *10,* 182.

[6] Cao, G.; Liu, D. Template-based synthesis of nanorod, nanowire, and nanotube arrays. *Adv. Colloid Interfac. Sci.* **2008,** *136,* 45–64.

[7] Satyanarayana, V. N. T.; Kuchibhatla, A. S.; Karakoti, D. B.; Seal, S. One dimensional nanostructured materials. *Prog. Mater. Sci.* **2007**, *52,* 699–691.

[8] Cornell, R. M.; Schwertmann, U. *The Iron Oxides*; VCH: Weinheim, 1996.

[9] Khedr, M. H.; Bahgat, M.; Nasr, M. I.; Sedeek, E. K. CO_2 decomposition over freshly reduced nanocrystalline Fe_2O_3. *Colloid. Surfaces A: Physicochem. Eng. Aspects* **2007,** *302,* 517–524.

[10] Chen, J.; Xu, L. N.; Li, W. Y.; Gou, X. L. alpha-Fe_2O_3 nanotubes in gas sensor and lithium-Ion battery applications. *Adv. Mater.* **2005,** *17,* 582–586.

[11] Brown, A. S. C.; Hargreaves, J. S. J.; Rijniersce, B. A study of the structural and catalytic effects of sulfation on iron oxide catalysts prepared from goethite and ferrihydrite precursors for methane oxidation. *Cat. Lett.* **1998,** *53,* 7–13

[12] Khare, N.; Eggleston, C. M.; Lovelace, D. M.; Boese, S. W. Structural and redox properties of mitochondrial cytochrome *c* co-sorbed with phosphate on hematite (alpha-Fe_2O_3) surfaces. *J. Colloid Interface Sci.* **2006,** *303,* 404–414.

[13] Srivastava, H.; Tiwari, P.; Srivastava, A. K; Nandedkar, R. V. Growth and characterization of alpha-Fe_2O_3 nanowires. *J. Appl. Phys.* **2007,** *102,* 054303.

[14] Dong, W. T.; Zhu, C. S. Use of ethylene oxide in the sol–gel synthesis of alpha-Fe_2O_3 nanoparticles from Fe(III) salts. *J. Mater. Chem.* **2002,** *12,* 1676–1683.

[15] Li, P.; Miser, D. E.; Rabiei, S.; Yadav, R. T.; Hajaligol, M. R. The removal of carbon monoxide by iron oxide nanoparticles. *Appl. Catal. B Env.* **2003,** *43,* 151–162.

[16] Chueh, Y. -L.; Lai, M. -W.; Liang, J. -Q.; Chou, L. -J.; Wang Z. L. Systematic study of the growth of aligned arrays of alpha-Fe_2O_3 and Fe_3O_4 nanowires by a vapor–solid process. *Adv. Funct. Mater.* **2006,** *16,* 2243–2251.

[17] Zhao, Y. M.; Li, Y. -H.; Ma, R. Z.; Roe, M. J.; McCartney, D. G.; Zhu, Y. Q. Growth and characterization of iron oxide nanorods/nanobelts prepared by a simple iron-water reaction. *Small* **2006,** *2,* 422–427.

[18] Qin, F.; Magtoto, N. P.; Garza, M.; Kelber, J. A. Oxide film growth on Fe(111) and scanning tunneling microscopy induced high electric field stress in Fe_2O_3/Fe(111). *Thin Solid Films* **2003,** *444,* 179–188.

[19] Han, Q.; Xu, Y. Y.; Fu, Y. Y.; Zhang, H.; Wang, R. M.; Wang, T. M.; Chen, Z. Y. Defects and growing mechanisms of α-Fe_2O_3 nanowires. *Chem. Phys. Lett.* **2006,** *431,* 100–103.

[20] Fu, Y. Y.; Wang, R. M.; Xu, J.; Chen, J.; Yan, Y.; Narlikar, A. V. Zhang, H. Synthesis of large arrays of aligned α-Fe_2O_3 nanowires. *Chem. Phys.Lett.* **2003,** *379,* 373–379.

[21] Wen, X.; Wang, S.; Ding, Y.; Wang, Z. L.; Yang, S. Controlled growth of large-area, uniform, vertically aligned arrays of α-Fe_2O_3 nanobelts and nanowires. *J. Phys. Chem. B* **2005,** *109,* 215–220.

[22] Takagi, R. Growth of oxide whiskers on metals at high

temperature. *J. Phys. Soc. Japan* **1957,** *12,* 1212–1218.

[23] Mozetic, M.; Cvelbar, U.; Sunkara, M. K.; Vaddiraju, S. A method for the rapid synthesis of large ouantities of metal oxide nanowires at low temperatures. *Adv. Mater.* **2005,** *17,* 2138–2142.

[24] Cvelbar, U.; Chen, Z.; Sunkara, M. K.; Mozetic, M. Spontaneous growth of superstructure α-Fe_2O_3 nanowire and nanobelt arrays in reactive oxygen Plasma. *Small* **2008,** *4,* 1610–1614.

[25] Aronniemi, M.; Sainio, J.; Lahtinen, J. Chemical state quantification of iron and chromium oxides using XPS: The effect of the background subtraction method. *Surface Sci.* **2005,** *578,* 108–123.

[26] Kawabe, T.; Shimomura, S.; Karasuda, T.; Tabata, K.; Suzuki, E.; Yamaguchi, Y. Photoemission study of dissociatively adsorbed methane on a pre-oxidized SnO_2 thin film. *Surf. Sci.* **2000,** *448,* 101–107.

[27] de Faria, D. L. A.; Lopes, F. N. Heated goethite and natural hematite: Can Raman spectroscopy be used to differentiate them? *Vib. Spectrosc.* **2007,** *45,*117–121.

[28] de Faria, D. L. A.; Silva, V.; de Oliveira, M. T. Raman microspectroscopy of some iron oxides and oxyhydroxides. *J. Raman Spectroscopy* **1997,** *28,* 873.

[30] Sato, Y.; Young, D. J. High-temperature corrosion of lron at 900 °C in atmospheres containing HCl and H_2O. *Oxid. Met.* **2001,** *55,* 243–260.

[31] Grosvenor, A. P.; Kobe, B. A.; McIntyre, N. S. Examination of the oxidation of iron by oxygen using X-ray photoelectron spectroscopy and QUASES (TM). *Surface Sci.* **2004,** *565,* 151–162.

[32] Pan, Z. W.; Dai, Z. R.; Wang, Z. L. Nanobelts of semiconducting oxides. *Science* **2001,** *291,* 1947–1949.

[33] Morales, A. M.; Lieber, C. M. A laser ablation method for the synthesis of crystalline semiconductor nanowires. *Science* **1998,** *279,* 208–211.

[34] Wagner, R. S.; Ellis, W. C. Vapor–liquid–solid mechanism of single crystal growth. *Appl. Phys. Lett.* **1964,** *4,* 89-90.

[35] Chueh, Y. L.; Lai, M. -W.; Liang, J. -Q.; Chou, L. -J.; Wang Z. L. Systematic study of the growth of aligned arrays of α-Fe_2O_3 and Fe_3O_4 nanowires by a vapor–solid process. *Adv. Funct. Mater.* **2006,** *16,* 2243–2251.

[36] Givargizov, E. I. Fundamental aspects of VLS growth. *J. Cryst. Growth* **1975,** *31,* 20–30.

[39] Raynaud, G. M.; Rapp, R. A. *In situ* observation of whiskers, pyramids and pits during the high-temperature oxidation of metals. *Oxid. Met.* **1984,** *21,* 89–102.

[40] Hiralal, P.; Unalan, H. E.; Wijayantha, K. G. U.; Kursumovic, A.; JefFerson, D .; MacManus-Driscoll, J. L.; Amaratunga, G. A. J. Growth and process conditions of aligned and patternable films of iron(III) oxide nanowires by thermal oxidation of iron. *Nanotechnology* **2008,** *19,* 455608.

[29] Saunders, S. R. J.; Monteiro, M.; Rizzo F. The oxidation behaviour of metals and alloys at high temperatures in atmospheres containing water vapour: A review. *Progress Mater. Sci.* **2008,** *53,* 775–837.

[37] Young, D. *High Temperature Oxidation and Corrosion of Metals*; Elsevier Corrosion Series: Oxford, 2008.

[38] Voss, D. A.; Butler, E. P.; Mitchell, T. E. The growth of hematite blades during the high-temperature oxidation of iron. *Metall. Trans. A* **1982**, *13A,* 929–935.